1986

Selection Considerations for Rotary Compressor Shaft Geometries

T. L. Kassouf

E. A. Tomayko

J. P. Vaccaro

SELECTION CONSIDERATIONS FOR ROTARY COMPRESSOR SHAFT GEOMETRIES

Thomas L. Kassouf
Program Manager

Edward A. Tomayko
Senior Engineer

Joseph P. Vaccaro
Senior Engineer

United Technologies, Carrier
P.O. Box 4803
Syracuse, New York 13221

ABSTRACT

Selection of shaft geometry is critical to the overall performance of a rotary compressor. Consideration is given to the development of rotary compressor shaft geometries to optimize efficiency and reliability.

The cylinder to piston dynamic clearance is of prime importance with respect to leakage losses. An analysis of bearing film thicknesses and shaft deflection was conducted to fully evaluate the impact of the clearance between cylinder and piston under operating conditions. Trade-offs between shaft stiffness and the impact on efficiency due to increasing component size is discussed.

The characteristic bearing edge loading found in rotary compressors is a major reliability concern. Examination of the causes of edge loading is made and design responses evaluated. Matching shaft stiffness to local bearing stiffness is critical.

Reliability and performance testing has confirmed the validity of the design approach selected.

DIMENSIONAL OPTIMIZATION

As rotary compressor technology becomes increasingly widespread, more is understood about the complex interrelationships between component geometries and factors such as efficiency, weight, machined surface area, bearing loads, vane P-V's, radiated noise, etc.

Each new rotary design represents an attempt to balance the various choices in order to most cost effectively meet the objectives established for the product.

To initially establish the base design of a rotary compressor, a computer model was created to develop and analyze alternate geometries for the various capacities under consideration. Figures 1.A and 1.B show schematics of the general construction of the rotary compressor. The model examined a number of cylinder bore to height ratios, as well as various bearing diameters. Based on previous investigations, limits were established for maximum vane P-V's and minimum rolling piston face widths T_p. A nondimensional loss function was established to facilitate evaluation of the leakage and heat transfer losses. The predicted response of the objective loss function to variation of cylinder bore and height while maintaining constant shaft diameters is shown in Figure 2 for an 18,000 btu/h compressor.

It is clearly seen from Figure 2 that it is desirable to minimize the diameter, $2R_c$, and height, H_c, of the cylinder in order to minimize leakage and heat transfer losses. In addition to providing for improvement in efficiency, the trend towards the reduction in pump component size commensurate with the decrease in cylinder diameter and height would result in lower costs. As is examined later, further benefits accrue from reducing the dimensions of the pump assembly associated with reductions in shaft deflection and bearing eccentricities.

The opportunity for continuing the size reduction of pump componentry is finally checked by many factors. The most key of these is the greater vane extension required to achieve the necessary pump displacement as the cylinder height and diameter are decreased. The greater vane travel during each revolution and hence greater acceleration associated with the large extension configurations leads to vane P-V's not sustainable without a decrease in reliability. Figure 3 delineates the tracking of average vane P-V's with the various geometries evaluated. Limiting the height reduction in addition to the vane P-V is the available space for the suction inlet. The diameter shrinkage is limited additionally by the minimum rolling piston face width T_p and minimum acceptable bearing diameters. A minimum piston face width is required to prevent excessive leakage to the suction chamber and the compression chamber (while still at intermediate pressure) from the

internal cavity of the piston which remains at discharge pressure. Minimum shaft dimensions are needed to provide adequate bearing surface for the support of internal loads and to achieve appropriate stiffness to prevent deflection acute enough to:

(a) allow contact with the bearing surfaces,

(b) allow contact between the piston and cylinder,

(c) allow contact between the motor rotor and stator.

Prototype Configuration

A first prototype, referred to herein as prototype A, was fabricated with conventional dimensions. Two successive prototypes, B and C, were built based on subsequent analysis and testing.

The three prototype cylinders considered are described in Table 1.

Table 1 Prototype Cylinder Dimensions

	Cyl Dia. (in)	Cyl Hgt. (in)
A	2.44	2.05
B	2.20	1.41
C	2.20	1.05

The three prototype eccentric shafts considered are described in Table 2.

Table 2 Prototype Eccentric Shaft Dimensions

	PEB Dia. (in)	ECC Dia. (in)	MEB Dia. (in)
A	1.00	1.51	1.00
B	0.86	1.36	0.94
C	0.86	1.36	0.94

The weights of the various pump assemblies, exclusive of motor and shell are given in Table 3.

Table 3 Prototype Pump Assembly Weights Less Shell and Motor

	Weight (lbs)
A	12.85
B	8.54
C	7.45

As can be seen, dramatic reductions in size and weight, and thus cost, can possibly be realized, but such reductions are not achievable without penalty. The impact of downsizing is considered with respect to shaft dimensions in particular.

ECCENTRIC SHAFT LOADS

The dynamic bearing loads for the pump end, motor end and eccentric bearings were calculated for several promising geometries. Initially, bearing loads were targeted to remain within the envelope found to be previously satisfactory for rotary compressors. For maximum enhancement of reliability it was desired to maintain the lowest bearing loads possible. The relationship among the forces involved is shown schematically in Figure 4. Derivations of the functions defining shaft loads for a rolling piston rotary compressor have appeared many times in the proceedings of this conference (Ref. [1,2,3]), and will not be repeated here. Incorporated into the bearing load analysis were the gas forces F_{pc}, vane tip forces F_{pn}, F_{pt}, and the inertial force F_{pi}. The coefficients of friction for the vane tip and vane sides were as reported in Reference [2].

Since the forces acting on the eccentric represent the summation of all the forces generated internal to the pump mechanism, those forces are shown for prototypes A, B and C in Figure 5. Figure 5, is a polar plot depicting the eccentric loads at an operating condition of P_s=55 PSIG, P_d=405 PSIG. The frame of reference for the plot is rotating relative to the cylinder, but fixed relative to the eccentric journal.

The differences among the forces generated within the alternate configurations are dramatic. The peak loads for design C being only 40% of those for design A. The dominant geometric variable impacting total bearing shaft loads is the height of the cylinder. Of course, a force reduction independent of a commensurate reduction in the bearing unit loadings and/or a reduction in shaft flexure is of little value.

DYNAMIC PISTON TO CYLINDER CLEARANCE

The radial clearance between the rolling piston and cylinder wall represents a major potential leakage loss. Generally, therefore, it is favorable to reduce the nominal clearance as much as possible without a resultant collision between the piston and the cylinder. There are many practical limitations to this reduction, such as machining tolerances. The comments below focus on the dynamic behavior of the clearance as a result of bearing eccentricity, discussed in Ref. [5], and shaft deflection.

Bearing Eccentricity Induced Displacement

The output from the dynamic load analysis was used to determine the various oil film thicknesses and the shaft journal trajectories. Using Booker's mobility method for the solution of dynamically loaded bearings [6], with correction of the oil film calculation as suggested by Goenka [7], the minimum oil film thicknesses, H_o, were developed for the pump, motor and eccentric bearings. The calculations of film thicknesses were conducted presuming maximum centered radial bearing clearances of 0.0004"/0.0005" and compressor operating conditions of P_s=55 PSIG, P_d=405 PSIG.

Radial displacements for the pump journal e_{pb}, rolling piston e_{eb}, and motor journal e_{mb} were then developed by multiplying the bearing eccentricities by the centered radial clearance. The compressors under study, per common practice, have larger motor bearings than pump bearings. Owing to the complexity of considering the tilting misalignment brought on by differential oil film thicknesses, the analysis was conducted presuming that the shaft was displaced evenly in both the pump and motor bearings, ie., $e_{pb} = e_{mb}$. As the pump bearing experiences a higher eccentricity, total shaft displacement was based on the pump journal trajectory.

Figure 6 illustrates the displacement of the center of the moveable member of a bearing system away from a concentric position with the stationary member (relative to a coordinate system fixed with respect to the concentric origin). In the case of the main bearings, the bearings are the fixed members while the journals are free to move within the bearing clearance. The rolling piston is the moveable member in the bearing system comprised of the piston and the eccentric shaft journal. Analysis of journal and piston motion within the bearing clearances does presume that all members involved are rigid bodies.

When displacements of the shaft and rolling piston are resolved along an axis normal to the tangent point between the rolling piston and the cylinder interior wall they are directly additive to the nominal clearance. This axis, X', is part of a rotating coordinate system fixed relative to the maximum eccentric point of the shaft.

The displacement of the piston clearance from a concentric trajectory due to the pump bearing eccentricity ranged from 41% to 54% of the displacement due to the eccentric bearing eccentricity. Shaft C realized a 30% reduction in pump bearing displacement over shaft A and a 10% reduction in eccentric bearing displacement.

Eccentric Shaft Deflection Induced Displacement

Once the displacement of the piston and shaft has been established, it becomes necessary to factor in the deflection of the shaft due to applied load in order to determine the total reduction in radial clearance between the piston and cylinder. An assumption was made that the shaft is supported at the mid-point of both the pump and motor end bearings.

The deflection was evaluated with a computer code written by one of the authors (Tomayko). It was determined, based on static testing with Prototype A, that there was excellent agreement between the results from the program and empirical data. The dominant feature affecting shaft deflection was found to be the length of the unsupported span. Shaft C was determined to afford a 68% reduction in deflection relative to Shaft A.

The trade-offs between increased shaft rigidity and component growth must be carefully weighed as was apparent from Figure 2. However, it should also be

realized that small changes in the diameters of critical sections could result in a dramatic increase in stiffness as the moment of inertia for circular sections increases proportionally to the fourth power of the radius. Therefore attention to the details of the configurations of transfer sections, grinding reliefs, and oil passages is of great value.

TOTAL VARIATION IN PISTON TO CYLINDER CLEARANCE

All of the components are now in place to determine the total dynamic variation in the piston to cylinder radial clearance. The total clearance deviation from the concentric clearance is given by summing the displacements of the pump journal, the piston, and the deflecting shaft:

$$\Delta C = e_{pb} + e_{eb} + \delta \qquad (1)$$

Starting with a base case of concentric positioning between the bearings and the cylinder, the residual radial clearance at any crank angle is given by:

$$C(\theta) = C_c - \Delta C(\theta) \qquad (2)$$

Obviously, a positive clearance change will result in a decreased final clearance while conversely, a negative change will increase the total clearance.

Clearance Trajectory Plots

Figures 7, 8, and 9 graphically illustrate the effect the impact of the individual contributors to clearance variation as well as the total deviation from a concentric trajectory for prototypes A, B, and C, respectively. The outermost circle in these trajectory plots represents the interior wall of the cylinder. Shown on a concentric origin with the cylinder wall is the trajectory that the minimum clearance point between piston and cylinder would take if all components were perfectly round, infinitely rigid and centered. This is nomenclatured as the concentric trajectory. The distance between the above described circles is proportional to the nominal radial clearance between the piston and the cylinder.

Trajectory excursions to the outside of the concentric line represent decreases in radial clearance. Excursions inside the concentric line represent increases in radial clearance. The deviations from the concentric path for the various trajectories

represented are scaled to the total clearance. In the case of Figures 7, 8 and 9, the nominal clearance is identical, therefore, the figures are all proportional.

It can be clearly seen that the impact on clearance can be ranked in descending order as follows:

(a) displacement of the rolling piston,
(b) displacement of the pump journal,
(c) deflection of the eccentric shaft.

Figure 10 compares the trajectories of C(θ) resulting from the combined displacements of bearings and shaft deflection for prototypes A, B and C. The differences in shaft dimensions result in significant variations in the clearance trajectory. The maximum C(θ) for prototype C is 17% less than for prototype A, while the minimum C(θ) is 24% greater for C than for A. The total variation in C(θ) during one revolution is 19% less for configuration C than for configuration A.

A tighter trajectory of the piston allows for the selection of reduced nominal clearance which can enhance efficiency through the reduction of leakage.

The trajectory plots have value in quickly illustrating the subrevolution variation in piston to cylinder radial clearance enabling the designer to make the most appropriate choice in deciding on the magnitude and direction of the eccentric assembly of the bearings to the cylinder.

EDGE LOADING

The phenomenon of bearing edge loading in rotary compressors has been well reported in the literature [8]. One widely employed method of eliminating the problem has been to relieve the edge of the bearing as illustrated in Figure 11. This is done to allow for enough elasticity in the bearing such that it tilts slightly under load assuming the same attitude as the shaft. Thus, a uniform thickness oil film can be maintained over the entire axial length of the bearing eliminating the edge loading problems. The disadvantage of using conventional machining techniques to fabricate this feature is the required width of the relief groove. The groove as it breachs the sealing face of the piston causes a constant high to low side leak. A partial intrusion of the groove across the sealing face reduces the effectivity of the seal if the residual width of the seal, T_p, falls below an experi-

mentally determined minimum. The net effect of placing a groove on the seal side of the bearing is to necessitate an increase in the outside diameter of the rolling piston. In turn the cylinder bore must be increased. These changes tend toward lower efficiency as shown previously in Figure 2.

A very narrow groove would minimize the trend towards growth of the other components, however, it is difficult to fabricate on a production basis. A first prototype was fabricated with no groove and experienced bearing distress after a short period under load. The addition of the narrow groove shown in Figure 12 alleviated the bearing distress problem. Of course it represented a low level of manufacturability.

It was postulated that the bearing nearly behaves as a plate with a reinforced center hole and that the main effect of the slot is to reduce the effective plate thickness. Experiment determined that the reduction in stiffness that the grooved bearing represented over the ungrooved plate was 28%. Thus, presuming that global flexibility of the bearing was critical, an alternate design bearing with the same stiffness as the grooved bearing was tested. The key feature needed for the alternate design was ease of manufacture. Proposed was a wider groove on the opposite cylinder side of the bearing as shown in Figure 13. The depth of the groove was chosen to achieve the same flexibility as the bearing in Figure 12. The width was chosen to give an L/D ratio of the groove allowing for conventional manufacturing processes such as high speed turning or net shape forming through the use of powdered metal.

Testing of bearings with the opposite cylinder side groove has proven eminently successful with no sacrifice in efficiency.

CONCLUSIONS

An evaluation was made of the sensitivity of the rotary compressor geometry to dimensional variation. Generally, it was determined that benefits result from maintaining the smallest pump size compatible with other limits.

The response of the bearing loads and shaft deflections to the reduced pump envelope was found to be favorable.

To visualize the dynamic piston to cylinder clearance, trajectory plots were generated which can aid in the appropriate selection of nominal clearance and assembly offset.

The characteristic edge loading found in rotary compressors was examined and alternative solutions analyzed. A satisfactory solution has been identified and verified.

LIST OF SYMBOLS

$C(\theta)$	Clearance between rolling piston and cylinder at shaft angle 0
E	Shaft eccentricity
e_{pb}	Displacement from center of the pump journal
e_{mb}	Displacement from center of the motor journal
e_{eb}	Displacement from center of the rolling piston
F_{pc}	Compression chamber gas force
F_{pi}	Rotating component inertial force
F_{pn}	Vane formal force
F_{pt}	Vane tangential force
F_{vd}	Vane gas force
F_{vi}	Vane inertial force
F_{vs}	Vane spring force
$F_{vsf1,2}$	Vane slot frictional forces
$F_{vsl1,2}$	Vane slot reaction forces
H_c	Cylinder height
H_o	Minimum bearing oil film thickness
L_g	Bearing relief groove depth
P_d	Discharge pressure
P_s	Suction pressure
R_c	Cylinder radius
T_g	Bearing relief groove width
T_p	Rolling piston sealing face width
w	Angular velocity of eccentric shaft
wp	Angular velocity of rolling piston
δ	Deflection of eccentric shaft
0	Shaft angle

REFERENCES

[1] Pandeya, P., Soedel, W., "Rolling Piston Type Rotary Compressors with special attention to friction and leakage", 1978 Purdue Compressor Technology Conference, p. 209.

[2] Yanagisawa, T., et al., "Motion Analysis of Rolling Piston in Rotary Compressor", 1982 Purdue Compressor Technology Conference, p. 185.

[3] Jorgensen, S.H., Nissen, H.S., "Mechanical Loss Model of Rolling Piston Rotary Compressor with Special Importance Attached to Journal Bearing:, 1984 Purdue Compressor Technology Conference, p. 323.

[4] Kawai, H., "Efficiency Improvement in Rolling Piston Type Rotary Compressors", 1984 Purdue Compressor Technology Conference, p. 299.

[5] Yanagisawa, T., Shimizu, T., "Leakage Losses with a Rolling Piston Type Rotary Compressor. I. Radial Clearance on the Rolling Piston", Revue Internationale du Froid, Volume 8, Numero 2, Mars 1985, p. 75.

[6] Booker, J.F., "Dynamically-Loaded Journal Bearings: Mobility Method of Solution", Trans. ASME, Journal of Basic Engineering, Vol. 87, Series D, Sept. 1965, p. 537.

[7] Goenka, P.K., "Analytical Curve Fits for Solution Parameters of Journal Bearings", GMR-4315, Mar. 18, 1983.

[8] Nomura, T., et al., "Efficiency Improvement in Rotary Compressor", 1984 Purdue Compressor Technology Conference, p. 307.

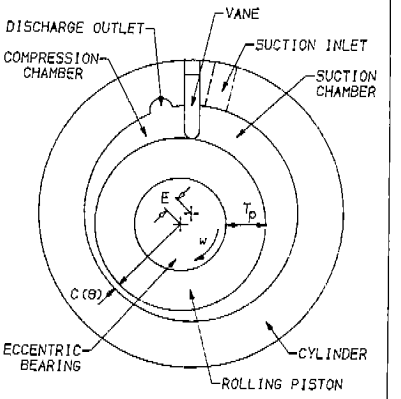

FIGURE 1.A
SCHEMATIC OF A ROLLING PISTON COMPRESSOR SECTION PERPENDICULAR TO THE ECCENTRIC SHAFT.

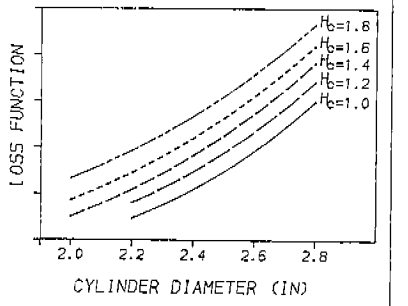

FIGURE 2
NON-DIMENSIONAL LOSS FUNCTION VS. CYLINDER HEIGHT AND DIAMETER FOR AN 18,000 BTU/H COMPRESSOR.

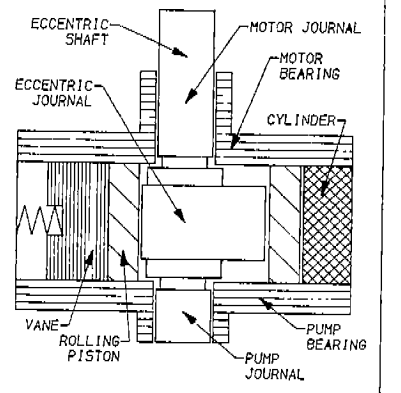

FIGURE 1.B
SCHEMATIC OF A ROLLING PISTON COMPRESSOR SECTION PARALLEL TO THE ECCENTRIC SHAFT.

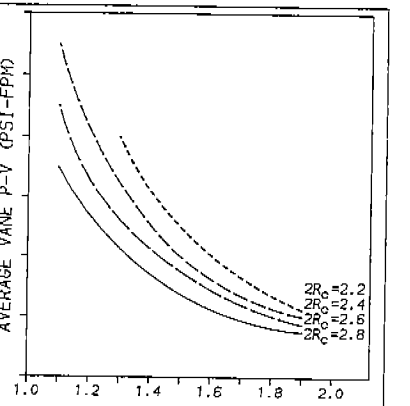

FIGURE 3
AVERAGE VANE P-V FOR VARIOUS 18,000 BTU/H GEOMETRIES.

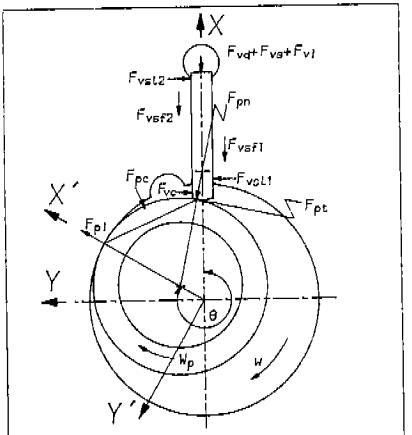

FIGURE 4
SCHEMATIC OF THE FORCES INVOLVED IN GENERATING THE BEARING LOAD.

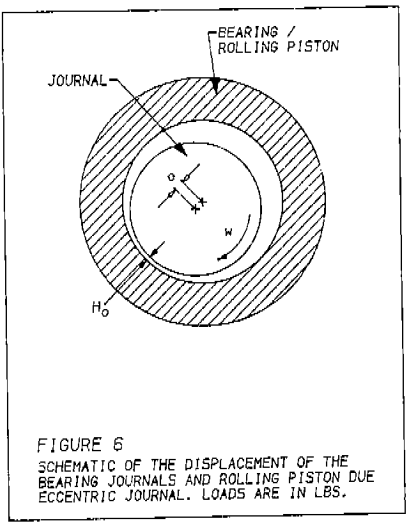

FIGURE 6
SCHEMATIC OF THE DISPLACEMENT OF THE BEARING JOURNALS AND ROLLING PISTON DUE ECCENTRIC JOURNAL. LOADS ARE IN LBS.

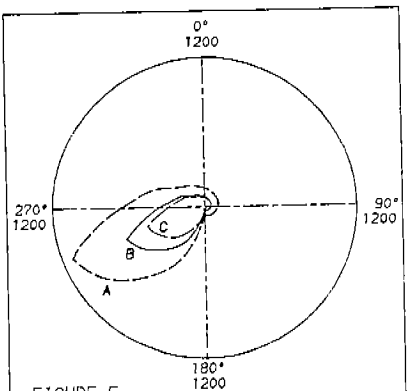

FIGURE 5
POLAR PLOT OF THE ECCENTRIC BEARING LOADS AT Ps = 55 PSIG, Pd = 405 PSIG FOR PROTOTYPES A, B, AND C. THE COORDINATE SYSTEM IS ROTATING RELATIVE TO THE CYLINDER, FIXED RELATIVE TO THE ECCENTRIC JOURNAL.

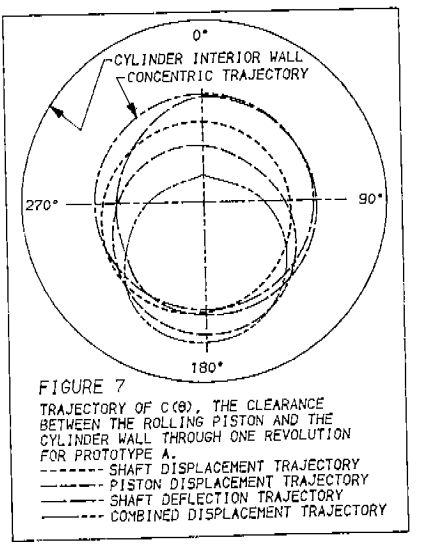

FIGURE 7
TRAJECTORY OF C(θ), THE CLEARANCE BETWEEN THE ROLLING PISTON AND THE CYLINDER WALL THROUGH ONE REVOLUTION FOR PROTOTYPE A.
- SHAFT DISPLACEMENT TRAJECTORY
- PISTON DISPLACEMENT TRAJECTORY
- SHAFT DEFLECTION TRAJECTORY
- COMBINED DISPLACEMENT TRAJECTORY

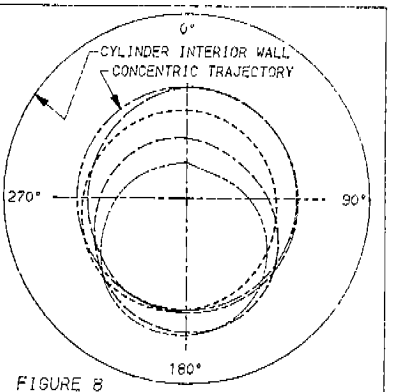

FIGURE 8

TRAJECTORY OF C(θ), THE CLEARANCE BETWEEN THE ROLLING PISTON AND THE CYLINDER WALL THROUGH ONE REVOLUTION FOR PROTOTYPE B.

- SHAFT DISPLACEMENT TRAJECTORY
- PISTON DISPLACEMENT TRAJECTORY
- SHAFT DEFLECTION TRAJECTORY
- COMBINED DISPLACEMENT TRAJECTORY

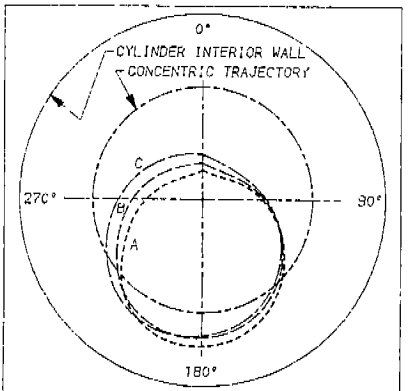

FIGURE 10

COMPARISON OF THE TRAJECTORIES OF C(θ) RESULTING FROM THE COMBINED DISPLACEMENTS OF BEARINGS AND SHAFT DEFLECTION, FOR PROTOTYPES A, B, AND C.

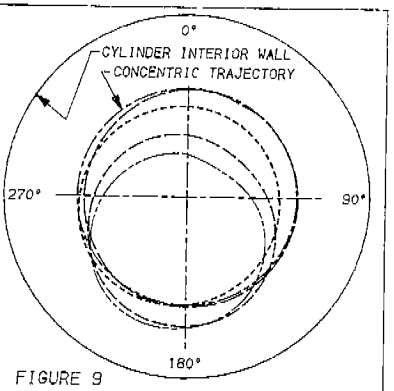

FIGURE 9

TRAJECTORY OF C(θ), THE CLEARANCE BETWEEN THE ROLLING PISTON AND THE CYLINDER WALL THROUGH ONE REVOLUTION FOR PROTOTYPE C.

- SHAFT DISPLACEMENT TRAJECTORY
- PISTON DISPLACEMENT TRAJECTORY
- SHAFT DEFLECTION TRAJECTORY
- COMBINED DISPLACEMENT TRAJECTORY

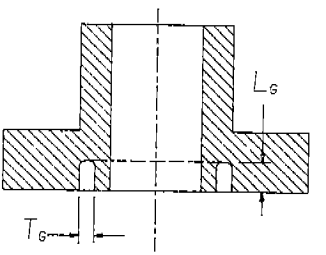

FIGURE 11

CROSS SECTION OF BEARING INCORPORATING A WIDE GROOVE ON SEALING FACE TO ALLOW FOR ALIGNMENT BETWEEN THE BEARING AND THE SHAFT.

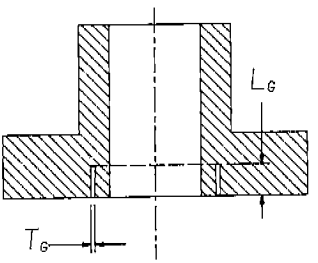

FIGURE 12
CROSS SECTION OF BEARING INCORPORATING
A NARROW GROOVE ON THE SEALING FACE.

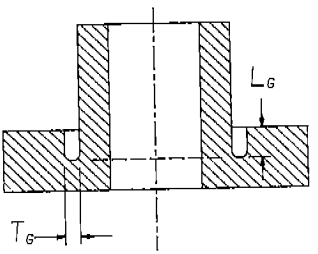

FIGURE 13
CROSS SECTION OF BEARING INCORPORATING
A WIDE GROOVE ON THE NON SEALING FACE.